Variational Multiscale Proper Orthogonal Decomposition: Navier-Stokes Equations

Traian Iliescu,[1] **Zhu Wang**[2]

[1] *Department of Mathematics, Virginia Polytechnic Institute and State University, Blacksburg, Virginia 24061-0123*

[2] *Institute for Mathematics and its Applications, University of Minnesota, Minneapolis, Minnesota 55455-0134*

Received 27 October 2012; accepted 30 September 2013
Published online 6 December 2013 in Wiley Online Library (wileyonlinelibrary.com).
DOI 10.1002/num.21835

We develop a variational multiscale proper orthogonal decomposition (POD) reduced-order model (ROM) for turbulent incompressible Navier-Stokes equations. Under two assumptions on the underlying finite element approximation and the generation of the POD basis, the error analysis of the full discretization of the ROM is presented. All error contributions are considered: the spatial discretization error (due to the finite element discretization), the temporal discretization error (due to the backward Euler method), and the POD truncation error. Numerical tests for a three-dimensional turbulent flow past a cylinder at Reynolds number $\mathrm{Re} = 1000$ show the improved physical accuracy of the new model over the standard Galerkin and mixing-length POD ROMs. The high computational efficiency of the new model is also showcased. Finally, the theoretical error estimates are confirmed by numerical simulations of a two-dimensional Navier-Stokes problem. Numer Methods Partial Differential Eq 30: 641–663, 2014

Keywords: finite element method; proper orthogonal decomposition; reduced-order model; variational multiscale

I. INTRODUCTION

Due to the complexity of fluid flows in many realistic engineering problems, millions or even billions of degrees of freedom are often required in a direct numerical simulation (DNS). To allow efficient numerical simulations in these applications, reduced-order models (ROMs) are often used. The proper orthogonal decomposition (POD) has been one of the most popular approaches used in developing ROMs for complex fluid flows [1–5]. It starts by using a DNS (or experimental data) to generate a POD basis $\{\boldsymbol{\varphi}_1, \ldots, \boldsymbol{\varphi}_d\}$ that maximizes the energy content in the system, where d is the rank of the data set. By utilizing the Galerkin method, one can project

Correspondence to: Zhu Wang, Institute for Mathematics and its Applications, University of Minnesota, Minneapolis, MN 55455-0134 (e-mail: wangzhu@ima.umn.edu)
Contract grant sponsor: National Science Foundation; contract grant numbers: DMS-0513542, OCE-0620464
Contract grant sponsor: Institute for Mathematics and its Applications (National Science Foundation)

the original system onto the space spanned by only a handful of dominant POD basis functions $\{\boldsymbol{\varphi}_1, \ldots, \boldsymbol{\varphi}_r\}$, with $r \leq d$, which results in a low-order model—the Galerkin projection-based POD-ROM (POD-G-ROM).

The POD-G-ROM has been applied successfully in the numerical simulation of laminar flows. It is well known, however, that a simple POD-G-ROM will generally produce erroneous results for turbulent flows [6]. The reason is that although the discarded POD modes $\{\boldsymbol{\varphi}_{r+1}, \ldots, \boldsymbol{\varphi}_d\}$ only contain a small part of the system's kinetic energy, they do, however, have a significant impact on the dynamics. To model the effect of the discarded POD modes, various approaches have been proposed (see, e.g., the survey in [7]). In this report, we develop an approach that improves the physical accuracy of the POD-ROM for turbulent incompressible fluid flows by utilizing a variational multiscale (VMS) idea [8, 9]. This method is an extension to the Navier-Stokes equations (NSE) of the VMS-POD-ROM that we proposed in [10] for convection-dominated convection-diffusion-reaction equations. Our approach uses an eddy viscosity (EV) to model the interaction between the discarded POD modes and those retained in the POD-ROM. Instead of being added to all the resolved POD modes $\{\boldsymbol{\varphi}_1, \ldots, \boldsymbol{\varphi}_r\}$, EV is only added to the small resolved scales (POD modes $\{\boldsymbol{\varphi}_{R+1}, \ldots, \boldsymbol{\varphi}_r\}$ with $R < r$) in the VMS-POD-ROM. Thus, the small scale oscillations are eliminated without polluting the large scale components of the approximation. The small scales in the VMS-POD-ROM are defined by a projection approach in [10], which is also used in [11–15] in the finite element (FE) context. We also note that a different approach was developed in [16, 17].

In this report, the VMS-POD-ROM is extended and studied for the NSE. Under two assumptions on the underlying FE approximation and the generation of the POD basis, the error analysis of the full discretization of the ROM (FE in space, backward Euler in time) is presented. A numerical test of the VMS-POD-ROM for a three-dimensional (3D) turbulent flow past a circular cylinder at Reynolds number $\mathrm{Re} = 1000$ is conducted to investigate the physical accuracy of the model. The theoretical error estimates are confirmed by using the VMS-POD-ROM in the numerical simulation of a two-dimensional (2D) flow.

The rest of this article is organized as follows: In Section II, we briefly describe the POD methodology and introduce the new VMS-POD-ROM. The error analysis for the full discretization of the new model is presented in Section III. The new methodology is tested numerically in Section IV for a 3D flow past a circular cylinder and a 2D flow problem. Finally, Section V presents the conclusions and future research directions.

II. VARIATIONAL MULTISCALE PROPER ORTHOGONAL DECOMPOSITION

We consider the numerical solution of the incompressible NSE:

$$\begin{cases} \mathbf{u}_t - \nu \Delta \mathbf{u} + (\mathbf{u} \cdot \nabla)\, \mathbf{u} + \nabla p = \mathbf{f}, & \text{in } \Omega \times (0, T], \\ \nabla \cdot \mathbf{u} = 0, & \text{in } \Omega \times (0, T], \\ \mathbf{u} = 0, & \text{on } \partial\Omega \times (0, T], \\ \mathbf{u}(\mathbf{x}, 0) = \mathbf{u}^0(\mathbf{x}), & \text{in } \Omega, \end{cases} \tag{2.1}$$

where $\mathbf{u}(\mathbf{x}, t)$ and $p(\mathbf{x}, t)$ represent the fluid velocity and pressure of a flow in the region Ω, respectively, for $\mathbf{x} \in \Omega$, $t \in [0, T]$, and $\Omega \subset \mathbb{R}^n$ with $n = 2$ or 3; the flow is bounded by walls and driven by the force $\mathbf{f}(\mathbf{x}, t)$; ν is the reciprocal of the Reynolds number; and $\mathbf{u}^0(\mathbf{x})$ denotes the initial velocity. We also assume that the boundary of the domain, $\partial\Omega$, is polygonal when $n = 2$ and is polyhedral when $n = 3$.

The following functional spaces and notations will be used in the article:

$$\mathbf{X} = \mathbf{H}_0^1(\Omega) = \left\{ \mathbf{v} \in [L^2(\Omega)]^n : \nabla \mathbf{v} \in [L^2(\Omega)]^{n\times n} \text{and } \mathbf{v} = 0 \text{ on } \partial\Omega \right\},$$

$$Q = L_0^2(\Omega) = \left\{ q \in L^2(\Omega) : \int_\Omega q \mathrm{d}\mathbf{x} = 0 \right\},$$

$$\mathbf{V} = \{ \mathbf{v} \in \mathbf{X} : (\nabla \cdot \mathbf{v}, q) = 0, \forall q \in Q \}, \text{and}$$

$$\mathbf{V}^h = \left\{ \mathbf{v}_h \in \mathbf{X}^h : (\nabla \cdot \mathbf{v}_h, q_h) = 0, \forall q_h \in Q^h \right\},$$

where $\mathbf{X}^h \subset \mathbf{X}$ and $Q^h \subset Q$ are the FE spaces of the velocity and pressure, respectively. In what follows, we consider the div-stable pair of FE spaces $\mathbb{P}^m/\mathbb{P}^{m-1}, m \geq 2$ [18]. That is, the FE approximation of the velocity is continuous on Ω and is an n-vector valued function with each component a polynomial of degree less than or equal to m when restricted to an element, while that of the pressure is also continuous on Ω and is a single valued function that is a polynomial of degree less than or equal to $m-1$ when restricted to an element. We emphasize, however, that our analysis extends to more general FE spaces. We consider the following spaces for the POD setting:

$$\mathbf{X}^r := \text{span} \left\{ \boldsymbol{\varphi}_1, \boldsymbol{\varphi}_2, \ldots, \boldsymbol{\varphi}_r \right\}, \tag{2.2a}$$

$$\mathbf{X}^R := \text{span} \left\{ \boldsymbol{\varphi}_1, \boldsymbol{\varphi}_2, \ldots, \boldsymbol{\varphi}_R \right\}, \text{and} \tag{2.2b}$$

$$\mathbf{L}^R := \text{span} \left\{ \nabla\boldsymbol{\varphi}_1, \nabla\boldsymbol{\varphi}_2, \ldots, \nabla\boldsymbol{\varphi}_R \right\}, \tag{2.2c}$$

where $\boldsymbol{\varphi}_j$, $j = 1, \ldots, r$, are the POD basis functions that will be defined in Section II.A. We note that $\mathbf{X}^R \subset \mathbf{X}^r$, since $R < r$.

We introduce the following notations: let $\mathcal{H}$ be a real Hilbert space endowed with inner product $(\cdot,\cdot)_{\mathcal{H}}$ and norm $||\cdot||_{\mathcal{H}}$. Let the trilinear form $b^*(\cdot,\cdot,\cdot)$ be defined as

$$b^*(\mathbf{u}, \mathbf{v}, \mathbf{w}) = \frac{1}{2} \left[((\mathbf{u} \cdot \nabla)\mathbf{v}, \mathbf{w}) - ((\mathbf{u} \cdot \nabla)\mathbf{w}, \mathbf{v}) \right]$$

and the norm $|||\cdot|||$ be defined as $|||\mathbf{v}|||_{s,k} := \left(\frac{1}{M} \sum_{i=0}^{M-1} ||\mathbf{v}(\cdot, t_{i+1})||_k^s \right)^{1/s}$, where s and M are positive integers.

The weak formulation of the NSE (2.1) reads: Find $\mathbf{u} \in \mathbf{X}$ and $p \in Q$ such that

$$\begin{cases} (\mathbf{u}_t, \mathbf{v}) + \nu(\nabla\mathbf{u}, \nabla\mathbf{v}) + b^*(\mathbf{u}, \mathbf{u}, \mathbf{v}) - (p, \nabla \cdot \mathbf{v}) = (\mathbf{f}, \mathbf{v}), & \forall \mathbf{v} \in \mathbf{X}, \\ (\nabla \cdot \mathbf{u}, q) = 0, & \forall q \in Q. \end{cases} \tag{2.3}$$

To ensure the uniqueness of the solution to (2.3), we make the following regularity assumptions (see Definition 29 and Remark 10 in [18]):

Assumption 2.1. *In (2.1), assume that* $\mathbf{f} \in L^2\left(0, T; \mathbf{L}^2(\Omega)\right)$, $\mathbf{u}^0 \in \mathbf{V}$, $\mathbf{u} \in L^2(0, T; \mathbf{X}) \cap L^\infty\left(0, T; \mathbf{L}^2(\Omega)\right)$, $\nabla\mathbf{u} \in \left(L^4\left(0, T; L^2(\Omega)\right)\right)^{n\times n}$, $\mathbf{u}_t \in L^2(0, T; \mathbf{X}^*)$, *and* $p \in L^2(0, T; Q)$.

The FE approximation of (2.3) can be written as follows: Find $\mathbf{u}_h \in \mathbf{V}^h$ such that

$$\left(\mathbf{u}_{h,t}, \mathbf{v}_h\right) + \nu(\nabla\mathbf{u}_h, \nabla\mathbf{v}_h) + b^*(\mathbf{u}_h, \mathbf{u}_h, \mathbf{v}_h) = (\mathbf{f}, \mathbf{v}_h), \forall \mathbf{v}_h \in \mathbf{V}^h \tag{2.4}$$

and $\mathbf{u}_h(\cdot, 0) = \mathbf{u}_h^0 \in \mathbf{V}^h$.

A. Proper Orthogonal Decomposition

We briefly describe the POD method, following [19]. For a detailed presentation, the reader is referred to [3, 20–23].

Consider an ensemble of snapshots $\mathcal{R} := \text{span}\{\mathbf{u}(\cdot,t_0),\ldots,\mathbf{u}(\cdot,t_M)\}$, which is a collection of velocity data from either numerical simulation results or experimental observations at time $t_i = i\Delta t$, $i = 0,\ldots,M$ and let $\Delta t = \frac{T}{M}$. The POD method seeks a low-dimensional basis $\{\boldsymbol{\varphi}_1,\ldots,\boldsymbol{\varphi}_r\}$ in $\mathcal{H}$ that optimally approximates the snapshots in the following sense:

$$\min \frac{1}{M+1}\sum_{\ell=0}^{M}\left\|\mathbf{u}(\cdot,t_\ell)-\sum_{j=1}^{r}\left(\mathbf{u}(\cdot,t_\ell),\boldsymbol{\varphi}_j(\cdot)\right)_{\mathcal{H}}\boldsymbol{\varphi}_j(\cdot)\right\|_{\mathcal{H}}^2 \tag{2.5}$$

subject to the conditions that $(\boldsymbol{\varphi}_j,\boldsymbol{\varphi}_i)_{\mathcal{H}} = \delta_{ij}, 1 \le i,j \le r$, where δ_{ij} is the Kronecker delta. To solve (2.5), one can consider the eigenvalue problem

$$K\mathbf{z}_j = \lambda_j \mathbf{z}_j, \text{ for } j = 1,\ldots,r, \tag{2.6}$$

where $K \in \mathbb{R}^{(M+1)\times(M+1)}$ is the snapshot correlation matrix with entries $K_{k\ell} = \frac{1}{M+1}(\mathbf{u}(\cdot,t_\ell),\mathbf{u}(\cdot,t_k))_{\mathcal{H}}$ for $\ell,k = 0,\ldots,M$, $\mathbf{z}_j$ is the j-th eigenvector, and λ_j is the associated eigenvalue. The eigenvalues are positive and sorted in descending order $\lambda_1 \ge \cdots \ge \lambda_r \ge 0$. It can then be shown that the solution of (2.5), the POD basis function, is given by

$$\boldsymbol{\varphi}_j(\cdot) = \frac{1}{\sqrt{\lambda_j}}\sum_{\ell=0}^{M}(\mathbf{z}_j)_\ell \mathbf{u}(\cdot,t_\ell), 1 \le j \le r, \tag{2.7}$$

where $(\mathbf{z}_j)_\ell$ is the ℓ-th component of the eigenvector $\mathbf{z}_j$. It can also be shown that the following error formula holds [19, 21]:

$$\frac{1}{M+1}\sum_{\ell=0}^{M}\left\|\mathbf{u}(\cdot,t_\ell)-\sum_{j=1}^{r}\left(\mathbf{u}(\cdot,t_\ell),\boldsymbol{\varphi}_j(\cdot)\right)_{\mathcal{H}}\boldsymbol{\varphi}_j(\cdot)\right\|_{\mathcal{H}}^2 = \sum_{j=r+1}^{d}\lambda_j, \tag{2.8}$$

where d is the rank of $\mathcal{R}$.

Remark 2.1. Since, as shown in (2.7), the POD basis functions are linear combinations of the snapshots, the POD basis functions satisfy the boundary conditions in (2.1) and are solenoidal. If the FE approximations are used as snapshots, the POD basis functions belong to $\mathbf{V}^h$, which yields $\mathbf{X}^r \subset \mathbf{V}^h$.

The Galerkin projection-based POD-ROM uses both Galerkin truncation and Galerkin projection. The former yields an approximation of the velocity field by a linear combination of the truncated POD basis:

$$\mathbf{u}(\mathbf{x},t) \approx \mathbf{u}_r(\mathbf{x},t) \equiv \sum_{j=1}^{r} a_j(t)\,\boldsymbol{\varphi}_j(\mathbf{x}), \tag{2.9}$$

where $\{a_j(t)\}_{j=1}^{r}$ are the sought time-varying coefficients representing the POD-Galerkin trajectories. Note that $r \ll N$, where N denotes the number of degrees of freedom in a DNS. Replacing

the velocity $\mathbf{u}$ with $\mathbf{u}_r$ in the NSE (2.1), using the Galerkin method, and projecting the resulted equations onto the space $\mathbf{X}^r$, one obtains the POD-G-ROM for the NSE: Find $\mathbf{u}_r \in \mathbf{X}^r$ such that

$$\left(\frac{\partial \mathbf{u}_r}{\partial t}, \boldsymbol{\varphi}\right) + \nu\left(\nabla \mathbf{u}_r, \nabla \boldsymbol{\varphi}\right) + b^*\left(\mathbf{u}_r, \mathbf{u}_r, \boldsymbol{\varphi}\right) = \left(\mathbf{f}, \boldsymbol{\varphi}\right), \forall \boldsymbol{\varphi} \in \mathbf{X}^r \tag{2.10}$$

and $\mathbf{u}_r(\cdot, 0) = \mathbf{u}_r^0 \in \mathbf{X}^r$. In (2.10), the pressure term vanishes due to the fact that all POD modes are solenoidal and satisfy the appropriate boundary conditions. The spatial and temporal discretizations of (2.10) were considered in [24, 25]. Despite its appealing computational efficiency, the POD-G-ROM (2.10) has generally been limited to laminar flows. To overcome this restriction, we develop a closure method for the POD-ROM, which stems from the VMS ideas.

B. Variational Multiscale Method

Based on the concept of energy cascade and locality of energy transfer, the VMS method models the effect of unresolved scales by introducing extra eddy viscosities to and only to the resolved small scales [8, 9]. For a standard FE discretization, the separation of scales is generally challenging. Indeed, unless special care is taken (e.g., mesh adaptivity is used), the FE basis does not include any a priori information regarding the scales displayed by the underlying problem. Since the POD basis functions are already listed in descending order of their kinetic energy content, the POD represents an ideal setting for the VMS methodology. Naturally, we regard the discarded POD basis functions as unresolved scales, $\{\boldsymbol{\varphi}_1, \ldots, \boldsymbol{\varphi}_R\}$ as resolved large scales, and $\{\boldsymbol{\varphi}_{R+1}, \ldots, \boldsymbol{\varphi}_r\}$ as resolved small scales, where $R < r$.

We consider the orthogonal projection of $\mathbf{L}^2$ on $\mathbf{L}^R$, $P_R : \mathbf{L}^2 \to \mathbf{L}^R$, defined by

$$\left(\mathbf{u} - P_R\mathbf{u}, \mathbf{v}_R\right) = 0, \quad \forall \mathbf{v}_R \in \mathbf{L}^R. \tag{2.11}$$

Let $P_R' := \mathbb{I} - P_R$, where $\mathbb{I}$ is the identity operator. We propose the *variational multiscale POD ROM (P_R-VMS-POD-ROM)* for the NSE: Find $\mathbf{u}_r \in \mathbf{X}^r$ such that

$$\left(\frac{\partial \mathbf{u}_r}{\partial t}, \boldsymbol{\varphi}\right) + \nu\left(\nabla \mathbf{u}_r, \nabla \boldsymbol{\varphi}\right) + b^*\left(\mathbf{u}_r, \mathbf{u}_r, \boldsymbol{\varphi}\right) + \alpha\left(P_R'\nabla \mathbf{u}_r, P_R'\nabla \boldsymbol{\varphi}\right) = \left(\mathbf{f}, \boldsymbol{\varphi}\right), \forall \boldsymbol{\varphi} \in \mathbf{X}^r, \tag{2.12}$$

where $\alpha > 0$ is a constant EV coefficient and the initial condition is given by the L^2 projection of $\mathbf{u}^0$ on $\mathbf{X}^r$:

$$\mathbf{u}_r(\cdot, 0) = \mathbf{u}_r^0 := \sum_{j=1}^{r} (\mathbf{u}^0, \boldsymbol{\varphi}_j)\boldsymbol{\varphi}_j. \tag{2.13}$$

Remark 2.2. When $R = r$ or $\alpha = 0$, the P_R-VMS-POD-ROM (2.12) coincides with the standard POD-G-ROM, since no EV is introduced. When $R = 0$, since EV is added to all modes in the POD-ROM, the P_R-VMS-POD-ROM (2.12) becomes the mixing-length POD-ROM (ML-POD-ROM) [6, 7]:

$$\left(\frac{\partial \mathbf{u}_r}{\partial t}, \boldsymbol{\varphi}\right) + \nu\left(\nabla \mathbf{u}_r, \nabla \boldsymbol{\varphi}\right) + b^*\left(\mathbf{u}_r, \mathbf{u}_r, \phi\right) + \alpha\left(\nabla \mathbf{u}_r, \nabla \boldsymbol{\varphi}\right) = \left(\mathbf{f}, \boldsymbol{\varphi}\right), \forall \boldsymbol{\varphi} \in \mathbf{X}^r. \tag{2.14}$$

Remark 2.3. We note that the P_R-VMS-POD-ROM (2.12) is different from the VMS-POD-ROM introduced in [7]. Indeed, the former uses the operator P_R' and a constant EV coefficient, whereas the later does not use the operator P_R' and uses a variable EV coefficient.

We consider the full discretization of (2.12): We use the backward Euler method with a time step Δt for the time integration and the FE space $\mathbb{P}^m$ with $m \geq 2$ and a mesh size h for the spatial discretization. For $k = 0, \ldots, M$, denote the approximation solution of (2.12) at $t_k = k\Delta t$ to be $\mathbf{u}_r^k = \mathbf{u}_{h,r}(t_k)$ and the force at t_k to be $\mathbf{f}^k = \mathbf{f}(t_k)$, respectively. Note that we have dropped the subscript "h" in $\mathbf{u}_r^k$ for clarity of notation. The discretized P_R -VMS-POD-ROM then reads: Find $\mathbf{u}_r^k \in \mathbf{X}^r$ such that

$$\left(\frac{\mathbf{u}_r^{k+1} - \mathbf{u}_r^k}{\Delta t}, \boldsymbol{\varphi}\right) + \nu\left(\nabla \mathbf{u}_r^{k+1}, \nabla \boldsymbol{\varphi}\right) + b^*\left(\mathbf{u}_r^{k+1}, \mathbf{u}_r^{k+1}, \boldsymbol{\varphi}\right) + \alpha\left(P_R' \nabla \mathbf{u}_r^{k+1}, P_R' \nabla \boldsymbol{\varphi}\right) = \left(\mathbf{f}^{k+1}, \boldsymbol{\varphi}\right), \quad \forall \boldsymbol{\varphi} \in \mathbf{X}^r, k = 0, \ldots, M-1 \tag{2.15}$$

with the initial condition given in (2.13): $\mathbf{u}_r^0 = \sum_{j=1}^r (\mathbf{u}^0, \boldsymbol{\varphi}_j)\boldsymbol{\varphi}_j$.

In the sequel, we denote by $\mathbf{u}^k$ and $\mathbf{u}_h^k$ the velocity solution of (2.3) and the FE velocity approximation of (2.4) at $t = t_k$, respectively.

III. ERROR ESTIMATES

In this section, we present the error analysis for the P_R -VMS-POD-ROM discretization (2.15). We take the FE solutions $\mathbf{u}_h(\cdot, t_i)$, $i = 1, \ldots, M$ as snapshots and choose $\mathcal{H} = L^2$ in the POD generation. The error source includes three main components: the spatial FE discretization error, the temporal discretization error, and the POD truncation error. We derive the error estimate in two steps. First, we gather some necessary assumptions and preliminary results in Section III.A. Then, we present the main result in Section III.B.

In the sequel, we assume C to be a generic constant, which varies in different places, but is always independent of the FE mesh size h, the FE order m, the eigenvalues λ_j and the time step size Δt.

A. Preliminaries

We will need the following results for developing a rigorous error estimate:

Assumption 3.1 (FE error)**.** *We assume that the FE approximation* $\mathbf{u}_h$ *of (2.4) satisfies the following error estimate:*

$$||\mathbf{u} - \mathbf{u}_h|| + h||\nabla(\mathbf{u} - \mathbf{u}_h)|| \leq C(h^{m+1} + \Delta t). \tag{3.16}$$

We also assume the following standard approximation property (see, e.g., page 166 in [18]):

$$\inf_{q_h \in Q^h} ||p - q_h|| \leq Ch^m. \tag{3.17}$$

Remark 3.1. In chapter V of [26], a linearized version of the implicit (backward) Euler scheme of the NSE (2.1) was considered (see Eq. (2.2)). Theorem 2.2 in the same chapter proves (optimal) first-order error estimates with respect to the time variable in the L^2 norm. On page 170, it is mentioned that the discretization with respect to the space variable is not considered, since it has already been thoroughly studied in chapter IV. In [27], the same linearized version of the implicit

(backward) Euler scheme as that in Eq. (2.2) in chapter V of [26] is considered. The theorem on page 44 in [27] proves (optimal) first-order error estimates with respect to the time variable in the H^1 norm. As in [26], the discretization with respect to the space variable was not considered. The implicit (backward) Euler scheme was also considered in [28]. Section "Time discretization" on page 765 in [28] outlines the derivation of an optimal error estimate with respect to both space and time under assumptions on the stability of the solution. We note that these assumptions are probably not valid in the fully turbulent regime considered in the numerical tests in Section IV. For the explicit (forward) Euler scheme, an (optimal) first-order error estimate with respect to the time variable was proven in [29]. Higher order schemes for the time discretization of the NSE were analyzed in [26, 30–32].

We note that the references cited earlier generally focus on proving error estimates for the L^2 norm of the error (i.e., the first term on the LHS of (3.16)). We also note that these references usually make assumptions regarding the regularity of the solution or the parameters of the numerical scheme. These assumptions are generally valid in laminar flow settings, but are usually not valid in realistic turbulent flow settings. Furthermore, even when they are valid, the dependency of the constants in the error estimates on the Reynolds number or the various norms of the solution renders these error estimates impractical for realistic turbulent flows. Finding robust numerical schemes for realistic turbulent flows is a fundamental problem that, to the best of our knowledge, is still open (see, e.g., the extensive discussion in [18, 33, 34]). The main goal of this report is, however, different. We are not aiming at developing robust numerical schemes for realistic turbulent flows. Instead, we assume that an acceptable scheme exists and we investigate whether the POD-ROM that we consider can achieve a similar numerical accuracy at a fraction of the computational cost. We emphasize that this approach is commonly used in the derivation of error estimates for POD-ROMs. Indeed, inequality (2.17) in Theorem 2.2 in [25] is similar to (although not the same as) inequality (3.16) in Assumption 3.1 of our report.

For the POD approximation, the following POD inverse estimate was proven in Lemma 2 in [19]:

Lemma 3.1. *Let $\boldsymbol{\varphi}_i$, $i = 1, \ldots, r$, be POD basis functions, M_r be the POD mass matrix with entries $[M_r]_{jk} = (\boldsymbol{\varphi}_k, \boldsymbol{\varphi}_j)$, and S_r be the POD stiffness matrix with entries $[S_r]_{jk} = [M_r]_{jk} + (\nabla\boldsymbol{\varphi}_k, \nabla\boldsymbol{\varphi}_j)$, where $j, k = 1, \ldots, r$. Let $||\cdot||_2$ denote the matrix 2-norm. Then, for all $\mathbf{v} \in \mathbf{X}^r$, the following estimates hold:*

$$||\mathbf{v}||_{L^2} \leq \sqrt{||M_r||_2||S_r^{-1}||_2}||\mathbf{v}||_{H^1}, \tag{3.18}$$

$$||\mathbf{v}||_{H^1} \leq \sqrt{||S_r||_2||M_r^{-1}||_2}||\mathbf{v}||_{L^2}. \tag{3.19}$$

Note that, since we chose $\mathcal{H} = L^2$ in the POD method, $||M_r||_2 = ||M_r^{-1}||_2 = 1$ in inequalities (3.18)–(3.19).

The L^2 norm of the POD projection error is given by (2.8) with $\mathcal{H} = L^2$. The H^1 norm of the POD projection error is given in the following lemma:

Lemma 3.2. *The POD projection error in the H^1 norm satisfies*

$$\frac{1}{M+1}\sum_{\ell=0}^{M}\left\|\mathbf{u}_h(\cdot,t_\ell) - \sum_{j=1}^{r}\left(\mathbf{u}_h(\cdot,t_\ell),\boldsymbol{\varphi}_j(\cdot)\right)\boldsymbol{\varphi}_j(\cdot)\right\|_1^2 = \sum_{j=r+1}^{d}||\boldsymbol{\varphi}_j||_1^2\lambda_j. \tag{3.20}$$

Note that the POD projection error for continuous functions, that is, the error in the $L^2(0,T;H^1(\Omega))$ norm, has been proven in [22] (Theorem 2, page 17). We consider the POD of a discrete function and derive the time averaged POD projection error in the H^1 norm as follows:

Proof. Let $Y = [\mathbf{u}_h(\cdot,t_0), \mathbf{u}_h(\cdot,t_1), \ldots, \mathbf{u}_h(\cdot,t_M)]$ be the snapshot matrix. A necessary optimality condition of the POD basis is given by the following eigenvalue problem (see, e.g., [35]):

$$\frac{1}{M+1} Y Y^{\intercal} \boldsymbol{\varphi}_j = \lambda_j \boldsymbol{\varphi}_j. \tag{3.21}$$

The POD projection error in the H^1 norm satisfies

$$\begin{aligned}
&\frac{1}{M+1}\sum_{\ell=0}^{M} \left\| \mathbf{u}_h(\cdot,t_\ell) - \sum_{j=1}^{r} \left(\mathbf{u}_h(\cdot,t_\ell), \boldsymbol{\varphi}_j(\cdot)\right) \boldsymbol{\varphi}_j(\cdot) \right\|_1^2 \\
&= \frac{1}{M+1}\sum_{\ell=0}^{M} \left\| \sum_{j=r+1}^{d} (\mathbf{u}_h(\cdot,t_\ell), \boldsymbol{\varphi}_j)\boldsymbol{\varphi}_j \right\|_1^2 \\
&= \frac{1}{M+1}\sum_{\ell=0}^{M} \left(\sum_{j=r+1}^{d} (\mathbf{u}_h(\cdot,t_\ell), \boldsymbol{\varphi}_j)\boldsymbol{\varphi}_j, \sum_{k=r+1}^{d} (\mathbf{u}_h(\cdot,t_\ell), \boldsymbol{\varphi}_k)\boldsymbol{\varphi}_k \right)_1 \\
&= \frac{1}{M+1}\sum_{\ell=0}^{M} \sum_{j=r+1}^{d} \sum_{k=r+1}^{d} (\mathbf{u}_h(\cdot,t_\ell), \boldsymbol{\varphi}_j)(\mathbf{u}_h(\cdot,t_\ell), \boldsymbol{\varphi}_k)(\boldsymbol{\varphi}_j, \boldsymbol{\varphi}_k)_1 \\
&= \sum_{j=r+1}^{d} \sum_{k=r+1}^{d} \left(\frac{1}{M+1}\sum_{\ell=0}^{M} (\mathbf{u}_h(\cdot,t_\ell), \boldsymbol{\varphi}_j)\mathbf{u}_h(\cdot,t_\ell), \boldsymbol{\varphi}_k \right) (\boldsymbol{\varphi}_j, \boldsymbol{\varphi}_k)_1 \\
&= \sum_{j=r+1}^{d} \sum_{k=r+1}^{d} \left(\frac{1}{M+1} Y Y^{\intercal} \boldsymbol{\varphi}_j, \boldsymbol{\varphi}_k \right) (\boldsymbol{\varphi}_j, \boldsymbol{\varphi}_k)_1 \\
&\overset{(3.21)}{=} \sum_{j=r+1}^{d} \sum_{k=r+1}^{d} \left(\lambda_j \boldsymbol{\varphi}_j, \boldsymbol{\varphi}_k \right) (\boldsymbol{\varphi}_j, \boldsymbol{\varphi}_k)_1 \\
&= \sum_{j=r+1}^{d} \sum_{k=r+1}^{d} \lambda_j \delta_{jk} (\boldsymbol{\varphi}_j, \boldsymbol{\varphi}_k)_1 = \sum_{j=r+1}^{d} \lambda_j ||\boldsymbol{\varphi}_j||_1^2,
\end{aligned} \tag{3.22}$$

which proves (3.20). ∎

We define the L^2 projection of $\mathbf{u}$, $P_r\mathbf{u}$, from $\mathbf{L}^2$ to $\mathbf{X}^r$ as follows:

$$\left(\mathbf{u} - P_r\mathbf{u}, \boldsymbol{\varphi}_r\right) = 0, \quad \forall \boldsymbol{\varphi}_r \in \mathbf{X}^r. \tag{3.23}$$

We have the following error estimate of the L^2 projection:

Lemma 3.3. *For any* $\mathbf{u}^k \in \mathbf{X}$ *, its* L^2 *projection,* $\mathbf{w}_r^k = P_r\mathbf{u}^k$ *, satisfies the following error estimates:*

$$\frac{1}{M+1}\sum_{k=0}^{M}\|\mathbf{u}^k-\mathbf{w}_r^k\|^2 \le C\left(h^{2m+2}+\Delta t^2+\sum_{j=r+1}^{d}\lambda_j\right), \tag{3.24}$$

$$\frac{1}{M+1}\sum_{k=0}^{M}\|\nabla\left(\mathbf{u}^k-\mathbf{w}_r^k\right)\|^2 \le C\left(h^{2m}+||S_r||_2h^{2m+2}+(1+||S_r||_2)\Delta t^2+\sum_{j=r+1}^{d}||\boldsymbol{\varphi}_j||_1^2\lambda_j\right). \tag{3.25}$$

Proof. By the definition of the L^2 projection (3.23), we have

$$\|\mathbf{u}^k-\mathbf{w}_r^k\|^2=\left(\mathbf{u}^k-\mathbf{w}_r^k,\mathbf{u}^k-\mathbf{w}_r^k\right)\overset{(3.23)}{=}\left(\mathbf{u}^k-\mathbf{w}_r^k,\mathbf{u}-\mathbf{v}_r^k\right),\quad \forall\mathbf{v}_r^k\in\mathbf{X}^r. \tag{3.26}$$

Using the Cauchy-Schwarz inequality in (3.26), we get

$$\|\mathbf{u}^k-\mathbf{w}_r^k\|\le||\mathbf{u}^k-\mathbf{v}_r^k||,\quad \forall\mathbf{v}_r^k\in\mathbf{X}^r. \tag{3.27}$$

Decompose $\mathbf{u}^k-\mathbf{v}_r^k=(\mathbf{u}^k-\mathbf{u}_h^k)+(\mathbf{u}_h^k-\mathbf{v}_r^k)$, where $\mathbf{u}_h^k$ is the corresponding FE approximation. Choosing $\mathbf{v}_r^k=P_r\mathbf{u}_h^k:=\sum_{j=1}^{r}\left(\mathbf{u}_h^k,\boldsymbol{\varphi}_j\right)\boldsymbol{\varphi}_j$ in (3.27), by the triangle inequality, Assumption 3.1, and the POD projection error estimate (2.8), we have

$$\begin{aligned}\frac{1}{M+1}\sum_{k=0}^{M}\|\mathbf{u}^k-\mathbf{w}_r^k\|^2 &\le \frac{1}{M+1}\sum_{k=0}^{M}\left(\|\mathbf{u}^k-\mathbf{u}_h^k\|+\|\mathbf{u}_h^k-P_r\mathbf{u}_h^k\|\right)^2\\ &\le C\left(h^{2m+2}+\Delta t^2+\sum_{j=r+1}^{d}\lambda_j\right),\end{aligned} \tag{3.28}$$

which proves error estimate (3.24).

Using the triangle inequality, Assumption 3.1, the POD inverse estimate (3.19) and Lemma 3.2, we obtain

$$\begin{aligned}&\frac{1}{M+1}\sum_{k=0}^{M}\|\nabla\left(\mathbf{u}^k-\mathbf{w}_r^k\right)\|^2\\ &\le \frac{1}{M+1}\sum_{k=0}^{M}\left(\|\nabla\left(\mathbf{u}^k-\mathbf{u}_h^k\right)\|+\|\nabla\left(\mathbf{u}_h^k-P_r\mathbf{u}_h^k\right)\|+\|\nabla\left(P_r\mathbf{u}_h^k-\mathbf{w}_r^k\right)\|\right)^2\\ &\le C\left(h^{2m}+\Delta t^2+\sum_{j=r+1}^{d}||\varphi_j||_1^2\lambda_j+||S_r||_2\frac{1}{M+1}\sum_{k=0}^{M}\|P_r\mathbf{u}_h^k-\mathbf{w}_r^k\|^2\right)\\ &\le C\left(h^{2m}+\Delta t^2+\sum_{j=r+1}^{d}||\varphi_j||_1^2\lambda_j+||S_r||_2\frac{1}{M+1}\sum_{k=0}^{M}\|\mathbf{u}_h^k-\mathbf{u}^k\|^2\right)\quad(\mathbf{w}_r^k=P_r\mathbf{u}^k)\\ &\le C\left(h^{2m}+||S_r||_2h^{2m+2}+(1+||S_r||_2)\Delta t^2+\sum_{j=r+1}^{d}||\boldsymbol{\varphi}_j||_1^2\lambda_j\right),\end{aligned} \tag{3.29}$$

which proves error estimate (3.25). ∎

We assume that the following estimates, which are similar to (3.24) and (3.25), are also valid:

Assumption 3.2. *For any $\mathbf{u}^k \in \mathbf{X}$, its L^2 projection, $\mathbf{w}_r^k = P_r\mathbf{u}^k$, satisfies the following error estimates:*

$$\|\mathbf{u}^k - \mathbf{w}_r^k\| \leq C\left(h^{m+1} + \Delta t + \sqrt{\sum_{j=r+1}^{d} \lambda_j}\right), \tag{3.30}$$

$$\|\nabla\left(\mathbf{u}^k - \mathbf{w}_r^k\right)\| \leq C\left(h^m + \sqrt{||S_r||_2}h^{m+1} + \sqrt{1 + ||S_r||_2}\Delta t + \sqrt{\sum_{j=r+1}^{d} ||\boldsymbol{\varphi}_j||_1^2 \lambda_j}\right). \tag{3.31}$$

Remark 3.2. The assumption that (3.30) and (3.31) hold is quite natural. It simply says that, in the POD truncation error formulas (2.8) and (3.20), no individual term is much larger than the other terms in the sums.

We also mention that formulas (3.30) and (3.31) would follow directly from the POD truncation error estimates (2.8) and (3.20) if we discarded the $\frac{1}{M+1}$ factor in those estimates. This could be accomplished simply by dropping the $\frac{1}{M+1}$ factor from the snapshot correlation matrix K. In fact, this approach is used in, for example, [24] (compare formula (3.5) in [24] with formula (2.8) in our report). We note, however, that by dropping the $\frac{1}{M+1}$ from the correlation matrix K would most likely increase the magnitudes of the eigenvalues on the RHS of the POD truncation error estimates (2.8) and (3.20).

Lemma 3.4 (see Lemma 13 and Lemma 14 in [18])**.** *For any functions $\mathbf{u}, \mathbf{v}, \mathbf{w} \in \mathbf{X}$, the skew-symmetric trilinear form $b^*(\cdot,\cdot,\cdot)$ satisfies*

$$b^*(\mathbf{u}, \mathbf{v}, \mathbf{v}) = 0, \tag{3.32}$$

$$b^*(\mathbf{u}, \mathbf{v}, \mathbf{w}) \leq C||\nabla\mathbf{u}||||\nabla\mathbf{v}||||\nabla\mathbf{w}||, \tag{3.33}$$

and a sharper bound

$$b^*(\mathbf{u}, \mathbf{v}, \mathbf{w}) \leq C\sqrt{||\mathbf{u}||||\nabla\mathbf{u}||}||\nabla\mathbf{v}||||\nabla\mathbf{w}||. \tag{3.34}$$

We have the following stability result for the P_R -VMS-POD-ROM (2.15):

Lemma 3.5. *The solution of (2.15) satisfies the following bound:*

$$\|\mathbf{u}_r^M\|^2 + \nu\Delta t \sum_{k=0}^{M-1} \|\nabla\mathbf{u}_r^{k+1}\|^2 \leq \|\mathbf{u}_r^0\|^2 + \frac{\Delta t}{\nu} \sum_{k=0}^{M-1} \|\mathbf{f}^{k+1}\|_{-1}^2. \tag{3.35}$$

Proof. Choosing $\boldsymbol{\varphi} := \mathbf{u}_r^{k+1}$ in (2.15) and noting that $b^*(\mathbf{u}_r^{k+1}, \mathbf{u}_r^{k+1}, \mathbf{u}_r^{k+1}) = 0$ by (3.32), we obtain

$$\left(\mathbf{u}_r^{k+1} - \mathbf{u}_r^k, \mathbf{u}_r^{k+1}\right) + \nu\Delta t\left(\nabla\mathbf{u}_r^{k+1}, \nabla\mathbf{u}_r^{k+1}\right) + \alpha\Delta t\left(P_R'\nabla\mathbf{u}_r^{k+1}, P_R'\nabla\mathbf{u}_r^{k+1}\right) = \Delta t\left(\mathbf{f}^{k+1}, \mathbf{u}_r^{k+1}\right). \tag{3.36}$$

Using the Cauchy-Schwarz inequality, Young's inequality and the fact that the last term on the LHS of (3.36) is positive yields

$$\frac{1}{2}\|\mathbf{u}_r^{k+1}\|^2 - \frac{1}{2}\|\mathbf{u}_r^{k}\|^2 + \nu\Delta t\|\nabla\mathbf{u}_r^{k+1}\|^2 \leq \Delta t\left(\mathbf{f}^{k+1}, \mathbf{u}_r^{k+1}\right). \tag{3.37}$$

Applying the Cauchy-Schwarz inequality and Young's inequality on the RHS of (3.37), we get

$$\frac{1}{2}\|\mathbf{u}_r^{k+1}\|^2 - \frac{1}{2}\|\mathbf{u}_r^{k}\|^2 + \nu\Delta t\|\nabla\mathbf{u}_r^{k+1}\|^2 \leq \frac{\Delta t}{2\nu}\|\mathbf{f}^{k+1}\|_{-1}^2 + \frac{\nu\Delta t}{2}\|\nabla\mathbf{u}_r^{k+1}\|^2. \tag{3.38}$$

Then, the stability estimate (3.35) follows by summing (3.38) from 0 to $M-1$. ∎

Lemma 3.6. *The a priori stability estimate in Lemma 3.5 yields the following bounds:*

$$||\mathbf{u}_r^{k+1}||^2 \leq \nu^{-1}|||\mathbf{f}|||_{2,-1}^2 + ||\mathbf{u}_r^0||^2, \quad \forall k = 0, \ldots, M-1. \tag{3.39}$$

B. Main Results

We are ready to derive the main result of this section, which provides the error estimates for the P_R -VMS-POD-ROM (2.15).

Theorem 3.1. *Under the regularity assumption of the exact solution (Assumption 2.1), the assumption on the FE approximation (Assumption 3.1) and the assumption on the POD projection error (Assumption 3.2), the solution of the P_R -VMS-POD-ROM (2.15) satisfies the following error estimate: There exists $\Delta t^* > 0$ such that the inequality*

$$\begin{aligned}
&\|\mathbf{u}^M - \mathbf{u}_r^M\|^2 + \nu\Delta t\sum_{k=0}^{M-1}\|\nabla\left(\mathbf{u}^{k+1} - \mathbf{u}_r^{k+1}\right)\|^2 \\
&\quad\leq C((1 + ||S_r||_2 + ||S_R||_2)\,\Delta t^2 + h^{2m} + (1 + ||S_r||_2 + ||S_R||_2)\,h^{2m+2} \\
&\qquad + \sum_{j=r+1}^{d}\left(1 + ||\boldsymbol{\varphi}_j||_1^2\right)\lambda_j + \sum_{j=R+1}^{d}||\boldsymbol{\varphi}_j||_1^2\lambda_j)
\end{aligned} \tag{3.40}$$

holds for all $\Delta t < \Delta t^*$.

Proof. We start deriving the error bound by splitting the error into two terms:

$$\mathbf{u}^{k+1} - \mathbf{u}_r^{k+1} = \left(\mathbf{u}^{k+1} - \mathbf{w}_r^{k+1}\right) - \left(\mathbf{u}_r^{k+1} - \mathbf{w}_r^{k+1}\right) = \boldsymbol{\eta}^{k+1} - \boldsymbol{\phi}_r^{k+1}. \tag{3.41}$$

The first term, $\boldsymbol{\eta}^{k+1} = \mathbf{u}^{k+1} - \mathbf{w}_r^{k+1}$, represents the difference between $\mathbf{u}^{k+1}$ and its L^2 projection on $\mathbf{X}^r$, which has been bounded in Lemma 3.3. The second term, $\boldsymbol{\phi}_r^{k+1}$, is the remainder.

Next, we construct the error equation. We first evaluate the weak formulation of the NSE (2.3) at $t = t^{k+1}$ and let $\mathbf{v} = \boldsymbol{\varphi}_r$, then subtract the P_R -VMS-POD-ROM (2.15) from it. We obtain

$$\begin{aligned}
&\left(\mathbf{u}_t^{k+1}, \boldsymbol{\varphi}_r\right) - \left(\frac{\mathbf{u}_r^{k+1} - \mathbf{u}_r^{k}}{\Delta t}, \boldsymbol{\varphi}_r\right) + \nu\left(\nabla\mathbf{u}^{k+1} - \nabla\mathbf{u}_r^{k+1}, \nabla\boldsymbol{\varphi}_r\right) + b^*\left(\mathbf{u}^{k+1}, \mathbf{u}^{k+1}, \boldsymbol{\varphi}_r\right) \\
&-b^*\left(\mathbf{u}_r^{k+1}, \mathbf{u}_r^{k+1}, \boldsymbol{\varphi}_r\right) - \left(p, \nabla\cdot\boldsymbol{\varphi}_r\right) - \alpha\left(P_R'\nabla\mathbf{u}_r^{k+1}, P_R'\nabla\boldsymbol{\varphi}_r\right) = 0, \quad \forall\boldsymbol{\varphi}_r \in \mathbf{X}^r.
\end{aligned} \tag{3.42}$$

By subtracting and adding the difference quotient term, $\left(\frac{\mathbf{u}^{k+1}-\mathbf{u}^{k}}{\Delta t}, \boldsymbol{\varphi}_r\right)$, in (3.42), and applying the decomposition (3.41), we have, for any $\boldsymbol{\varphi}_r \in \mathbf{X}^r$,

$$\begin{aligned}
&\left(\mathbf{u}_t^{k+1} - \frac{\mathbf{u}^{k+1}-\mathbf{u}^{k}}{\Delta t}, \boldsymbol{\varphi}_r\right) + \frac{1}{\Delta t}\left(\boldsymbol{\eta}^{k+1} - \boldsymbol{\phi}_r^{k+1}, \boldsymbol{\varphi}_r\right) - \frac{1}{\Delta t}\left(\boldsymbol{\eta}^{k} - \boldsymbol{\phi}_r^{k}, \boldsymbol{\varphi}_r\right) \\
&\quad + \nu\left(\nabla\left(\boldsymbol{\eta}^{k+1} - \boldsymbol{\phi}_r^{k+1}\right), \nabla\boldsymbol{\varphi}_r\right) + b^*\left(\mathbf{u}^{k+1}, \mathbf{u}^{k+1}, \boldsymbol{\varphi}_r\right) - b^*\left(\mathbf{u}_r^{k+1}, \mathbf{u}_r^{k+1}, \boldsymbol{\varphi}_r\right) \\
&\quad - \left(p, \nabla\cdot\boldsymbol{\varphi}_r\right) - \alpha\left(P_R'\nabla\mathbf{u}_r^{k+1}, P_R'\nabla\boldsymbol{\varphi}_r\right) = 0.
\end{aligned} \tag{3.43}$$

Note that (3.23) implies that $\left(\boldsymbol{\eta}^{k}, \boldsymbol{\varphi}_r\right) = 0$ and $\left(\boldsymbol{\eta}^{k+1}, \boldsymbol{\varphi}_r\right) = 0$. Choosing $\boldsymbol{\varphi}_r = \boldsymbol{\phi}_r^{k+1}$ in (3.43) and letting $\mathbf{r}^k = \mathbf{u}_t^{k+1} - \frac{\mathbf{u}^{k+1}-\mathbf{u}^{k}}{\Delta t}$, we obtain

$$\begin{aligned}
&\frac{1}{\Delta t}\left(\boldsymbol{\phi}_r^{k+1}, \boldsymbol{\phi}_r^{k+1}\right) - \frac{1}{\Delta t}\left(\boldsymbol{\phi}_r^{k}, \boldsymbol{\phi}_r^{k+1}\right) + \nu\left(\nabla\boldsymbol{\phi}_r^{k+1}, \nabla\boldsymbol{\phi}_r^{k+1}\right) \\
&\quad = \left(\mathbf{r}^k, \boldsymbol{\phi}_r^{k+1}\right) + \nu\left(\nabla\boldsymbol{\eta}^{k+1}, \nabla\boldsymbol{\phi}_r^{k+1}\right) + b^*\left(\mathbf{u}^{k+1}, \mathbf{u}^{k+1}, \boldsymbol{\phi}_r^{k+1}\right) \\
&\qquad - b^*\left(\mathbf{u}_r^{k+1}, \mathbf{u}_r^{k+1}, \boldsymbol{\phi}_r^{k+1}\right) - \left(p, \nabla\cdot\boldsymbol{\phi}_r^{k+1}\right) - \alpha\left(P_R'\nabla\mathbf{u}_r^{k+1}, P_R'\nabla\boldsymbol{\phi}_r^{k+1}\right).
\end{aligned} \tag{3.44}$$

First, we estimate the LHS of (3.44) by applying the Cauchy-Schwarz inequality and Young's inequality:

$$\begin{aligned}
\text{LHS} &= \frac{1}{\Delta t}\|\boldsymbol{\phi}_r^{k+1}\|^2 - \frac{1}{\Delta t}\left(\boldsymbol{\phi}_r^{k}, \boldsymbol{\phi}_r^{k+1}\right) + \nu\|\nabla\boldsymbol{\phi}_r^{k+1}\|^2 \\
&\geq \frac{1}{2\Delta t}\left(\|\boldsymbol{\phi}_r^{k+1}\|^2 - \|\boldsymbol{\phi}_r^{k}\|^2\right) + \nu\|\nabla\boldsymbol{\phi}_r^{k+1}\|^2.
\end{aligned} \tag{3.45}$$

Multiplying by $2\Delta t$ both sides of inequality (3.45) and using the result in (3.44), we obtain

$$\begin{aligned}
&\|\boldsymbol{\phi}_r^{k+1}\|^2 - \|\boldsymbol{\phi}_r^{k}\|^2 + 2\nu\Delta t\|\nabla\boldsymbol{\phi}_r^{k+1}\|^2 \\
&\quad \leq 2\Delta t\left(\mathbf{r}^k, \boldsymbol{\phi}_r^{k+1}\right) + 2\nu\Delta t\left(\nabla\boldsymbol{\eta}^{k+1}, \nabla\boldsymbol{\phi}_r^{k+1}\right) + 2\Delta t b^*\left(\mathbf{u}^{k+1}, \mathbf{u}^{k+1}, \boldsymbol{\phi}_r^{k+1}\right) \\
&\qquad - 2\Delta t b^*\left(\mathbf{u}_r^{k+1}, \mathbf{u}_r^{k+1}, \boldsymbol{\phi}_r^{k+1}\right) - 2\Delta t\left(p, \nabla\cdot\boldsymbol{\phi}_r^{k+1}\right) - 2\alpha\Delta t\left(P_R'\nabla\mathbf{u}_r^{k+1}, P_R'\nabla\boldsymbol{\phi}_r^{k+1}\right).
\end{aligned} \tag{3.46}$$

Next, we estimate the terms on the RHS of (3.46) one by one. Using the Cauchy-Schwarz inequality and Young's inequality, we get

$$\left(\mathbf{r}^k, \boldsymbol{\phi}_r^{k+1}\right) \leq \|\mathbf{r}^k\|_{-1}\|\nabla\boldsymbol{\phi}_r^{k+1}\| \leq \frac{c_1^{-1}}{4}\|\mathbf{r}^k\|_{-1}^2 + c_1\|\nabla\boldsymbol{\phi}_r^{k+1}\|^2, \tag{3.47}$$

$$\nu\left(\nabla\boldsymbol{\eta}^{k+1}, \nabla\boldsymbol{\phi}_r^{k+1}\right) \leq \nu\|\nabla\boldsymbol{\eta}^{k+1}\|\|\nabla\boldsymbol{\phi}_r^{k+1}\| \leq \frac{c_2^{-1}\nu}{4}\|\nabla\boldsymbol{\eta}^{k+1}\|^2 + c_2\nu\|\nabla\boldsymbol{\phi}_r^{k+1}\|^2. \tag{3.48}$$

The nonlinear terms in (3.46) can be written as follows:

$$\begin{aligned}
&b^*\left(\mathbf{u}^{k+1}, \mathbf{u}^{k+1}, \boldsymbol{\phi}_r^{k+1}\right) - b^*\left(\mathbf{u}_r^{k+1}, \mathbf{u}_r^{k+1}, \boldsymbol{\phi}_r^{k+1}\right) \\
&\quad = b^*\left(\mathbf{u}_r^{k+1}, \boldsymbol{\eta}^{k+1} - \boldsymbol{\phi}_r^{k+1}, \boldsymbol{\phi}_r^{k+1}\right) + b^*\left(\boldsymbol{\eta}^{k+1} - \boldsymbol{\phi}_r^{k+1}, \mathbf{u}^{k+1}, \boldsymbol{\phi}_r^{k+1}\right) \\
&\quad = b^*\left(\mathbf{u}_r^{k+1}, \boldsymbol{\eta}^{k+1}, \boldsymbol{\phi}_r^{k+1}\right) + b^*\left(\boldsymbol{\eta}^{k+1}, \mathbf{u}^{k+1}, \boldsymbol{\phi}_r^{k+1}\right) - b^*\left(\boldsymbol{\phi}_r^{k+1}, \mathbf{u}^{k+1}, \boldsymbol{\phi}_r^{k+1}\right),
\end{aligned} \tag{3.49}$$

where we have used $b^*\left(\mathbf{u}^{k+1}, \phi_r^{k+1}, \phi_r^{k+1}\right) = 0$, which follows from (3.32). Next, we estimate each term on the RHS of (3.49). Since $\mathbf{u}_r^{k+1}, \boldsymbol{\eta}^{k+1}, \phi_r^{k+1} \in \mathbf{X}$, we can apply the standard bounds for the trilinear form $b^*(\cdot,\cdot,\cdot)$ and use Young's inequality:

$$
\begin{aligned}
b^*\left(\mathbf{u}_r^{k+1}, \boldsymbol{\eta}^{k+1}, \phi_r^{k+1}\right) &\overset{(3.34)}{\leq} C\|\mathbf{u}_r^{k+1}\|^{1/2}\|\nabla\mathbf{u}_r^{k+1}\|^{1/2}\|\nabla\boldsymbol{\eta}^{k+1}\|\|\nabla\phi_r^{k+1}\| \\
&\leq \frac{1}{4c_3}C^2\|\mathbf{u}_r^{k+1}\|\|\nabla\mathbf{u}_r^{k+1}\|\|\nabla\boldsymbol{\eta}^{k+1}\|^2 + c_3\|\nabla\phi_r^{k+1}\|^2; \qquad (3.50) \\
b^*\left(\boldsymbol{\eta}^{k+1}, \mathbf{u}^{k+1}, \phi_r^{k+1}\right) &\overset{(3.33)}{\leq} C\|\nabla\boldsymbol{\eta}^{k+1}\|\|\nabla\mathbf{u}^{k+1}\|\|\nabla\phi_r^{k+1}\| \\
&\leq \frac{1}{4c_4}C^2\|\nabla\mathbf{u}^{k+1}\|^2\|\nabla\boldsymbol{\eta}^{k+1}\|^2 + c_4\|\nabla\phi_r^{k+1}\|^2; \qquad (3.51) \\
b^*\left(\phi_r^{k+1}, \mathbf{u}^{k+1}, \phi_r^{k+1}\right) &\overset{(3.34)}{\leq} C\|\phi_r^{k+1}\|^{\frac{1}{2}}\|\nabla\phi_r^{k+1}\|^{\frac{1}{2}}\|\nabla\mathbf{u}^{k+1}\|\|\nabla\phi_r^{k+1}\| \\
&= C\|\phi_r^{k+1}\|^{\frac{1}{2}}\|\nabla\mathbf{u}^{k+1}\|\|\nabla\phi_r^{k+1}\|^{\frac{3}{2}} \\
&\leq C\frac{c_5^{-3}}{4}\|\nabla\mathbf{u}^{k+1}\|^4\|\phi_r^{k+1}\|^2 + C\frac{3c_5}{4}\|\nabla\phi_r^{k+1}\|^2. \qquad (3.52)
\end{aligned}
$$

Since $\phi_r^{k+1} \in \mathbf{X}^r \subset \mathbf{V}^h$, the pressure term on the RHS of (3.46) can be written as

$$
-\left(p, \nabla\cdot\phi_r^{k+1}\right) = -\left(p - q_h, \nabla\cdot\phi_r^{k+1}\right), \qquad (3.53)
$$

where q_h is any function in Q^h. Thus, the pressure term can be estimated as follows by the Cauchy-Schwarz inequality and Young's inequality:

$$
-\left(p, \nabla\cdot\phi_r^{k+1}\right) \leq \frac{1}{4c_6}\|p - q_h\|^2 + c_6\|\nabla\phi_r^{k+1}\|^2. \qquad (3.54)
$$

The last term on the RHS of (3.46) can be estimated as follows:

$$
\begin{aligned}
&-\alpha\left(P_R'\nabla\mathbf{u}_r^{k+1}, P_R'\nabla\phi_r^{k+1}\right) \\
&= \alpha\left(P_R'\nabla\mathbf{u}^{k+1} - P_R'\nabla\mathbf{u}_r^{k+1}, P_R'\nabla\phi_r^{k+1}\right) - \alpha\left(P_R'\nabla\mathbf{u}^{k+1}, P_R'\nabla\phi_r^{k+1}\right) \\
&= \alpha\left(P_R'\nabla\boldsymbol{\eta}^{k+1}, P_R'\nabla\phi_r^{k+1}\right) - \alpha\left(P_R'\nabla\phi_r^{k+1}, P_R'\nabla\phi_r^{k+1}\right) - \alpha\left(P_R'\nabla\mathbf{u}^{k+1}, P_R'\nabla\phi_r^{k+1}\right) \\
&\leq \alpha\|P_R'\nabla\boldsymbol{\eta}^{k+1}\|\cdot\|P_R'\nabla\phi_r^{k+1}\| - \alpha\|P_R'\nabla\phi_r^{k+1}\|^2 - \alpha\left(P_R'\nabla\mathbf{u}^{k+1}, P_R'\nabla\phi_r^{k+1}\right) \\
&\leq \alpha\left(\|P_R'\nabla\boldsymbol{\eta}^{k+1}\|^2 + \frac{1}{4}\|P_R'\nabla\phi_r^{k+1}\|^2\right) - \alpha\|P_R'\nabla\phi_r^{k+1}\|^2 + \alpha\left(\|P_R'\nabla\mathbf{u}^{k+1}\|^2 + \frac{1}{4}\|P_R'\nabla\phi_r^{k+1}\|^2\right) \\
&\leq \alpha\|P_R'\nabla\boldsymbol{\eta}^{k+1}\|^2 - \frac{\alpha}{2}\|P_R'\nabla\phi_r^{k+1}\|^2 + \alpha\|P_R'\nabla\mathbf{u}^{k+1}\|^2. \qquad (3.55)
\end{aligned}
$$

Note that, since P_R is the L^2 projection of $\mathbf{L}^2$ on $\mathbf{L}^R$, we get

$$
\|P_R'\nabla\boldsymbol{\eta}^{k+1}\| \leq \|\nabla\boldsymbol{\eta}^{k+1}\|.
$$

Choosing $c_1 = c_3 = c_4 = c_6 = \frac{\nu}{12}$, $c_2 = \frac{1}{12}$ and $c_5 = \frac{\nu}{9C}$, then substituting the above inequalities in (3.46), we obtain

$$\begin{aligned}
&\|\phi_r^{k+1}\|^2 - \|\phi_r^k\|^2 + \nu\Delta t\|\nabla\phi_r^{k+1}\|^2 + \alpha\Delta t\|P_R'\nabla\phi_r^{k+1}\|^2 \\
&\quad\le \frac{6\Delta t}{\nu}\|\mathbf{r}^k\|_{-1}^2 + 6\nu\Delta t\|\nabla\boldsymbol{\eta}^{k+1}\|^2 + \frac{6\Delta t}{\nu}C^2\|\mathbf{u}_r^{k+1}\|\|\nabla\mathbf{u}_r^{k+1}\|\|\nabla\boldsymbol{\eta}^{k+1}\|^2 \\
&\quad + \frac{6\Delta t}{\nu}C^2\|\nabla\mathbf{u}^{k+1}\|^2\|\nabla\boldsymbol{\eta}^{k+1}\|^2 + \frac{C^4 9^3\nu^{-3}\Delta t}{2}\|\nabla\mathbf{u}^{k+1}\|^4\|\phi_r^{k+1}\|^2 + \frac{6\Delta t}{\nu}\|p - q_h\|^2 \\
&\quad + 2\alpha\Delta t\|\nabla\boldsymbol{\eta}^{k+1}\|^2 + 2\alpha\Delta t\|P_R'\nabla\mathbf{u}^{k+1}\|^2. \qquad (3.56)
\end{aligned}$$

Summing (3.56) from $k=0$ to $k = M-1$, we have

$$\begin{aligned}
&\|\phi_r^M\|^2 + \nu\Delta t\sum_{k=0}^{M-1}\|\nabla\phi_r^{k+1}\|^2 + \alpha\Delta t\sum_{k=0}^{M-1}\|P_R'\nabla\phi_r^{k+1}\|^2 \\
&\le \|\phi_r^0\|^2 + \frac{6\Delta t}{\nu}\sum_{k=0}^{M-1}\|\mathbf{r}^k\|_{-1}^2 + 6\nu\Delta t\sum_{k=0}^{M-1}\|\nabla\boldsymbol{\eta}^{k+1}\|^2 + \frac{6\Delta t}{\nu}C^2\sum_{k=0}^{M-1}\|\mathbf{u}_r^{k+1}\|\|\nabla\mathbf{u}_r^{k+1}\|\|\nabla\boldsymbol{\eta}^{k+1}\|^2 \\
&\quad + \frac{6\Delta t}{\nu}C^2\sum_{k=0}^{M-1}\|\nabla\mathbf{u}^{k+1}\|^2\|\nabla\boldsymbol{\eta}^{k+1}\|^2 + \frac{C^4 9^3\nu^{-3}\Delta t}{2}\sum_{k=0}^{M-1}\|\nabla\mathbf{u}^{k+1}\|^4\|\phi_r^{k+1}\|^2 \\
&\quad + \frac{6\Delta t}{\nu}\sum_{k=0}^{M-1}\|p - q_h\|^2 + 2\alpha\Delta t\sum_{k=0}^{M-1}\|\nabla\boldsymbol{\eta}^{k+1}\|^2 + 2\alpha\Delta t\sum_{k=0}^{M-1}\|P_R'\nabla\mathbf{u}^{k+1}\|^2. \qquad (3.57)
\end{aligned}$$

Next, we estimate each term on the RHS of (3.57).

The first term vanishes since $\mathbf{u}_r^0 = \mathbf{w}_r^0$ (see (2.13)).

By using the Poincaré-Friedrichs inequality, the second term on the RHS of (3.57) can be estimated as follows (see, e.g., [10]):

$$\Delta t\sum_{k=0}^{M-1}\|\mathbf{r}^k\|_{-1}^2 \le C\Delta t\sum_{k=0}^{M-1}\|\mathbf{r}^k\|^2 \le C\Delta t^2\|\mathbf{u}_{tt}\|_{2,2}^2. \qquad (3.58)$$

Using (3.25), the third and eighth terms on the RHS of (3.57) can be estimated as follows:

$$\Delta t\sum_{k=0}^{M-1}\|\nabla\boldsymbol{\eta}^{k+1}\|^2 \le C\left(h^{2m} + ||S_r||_2 h^{2m+2} + (1 + ||S_r||_2)\,\Delta t^2 + \sum_{j=r+1}^{d}||\boldsymbol{\varphi}_j||_1^2\lambda_j\right). \qquad (3.59)$$

To estimate the fourth term on the RHS of (3.57), we use Lemma 3.6

$$\begin{aligned}
&\Delta t\sum_{k=0}^{M-1}\|\mathbf{u}_r^{k+1}\|\|\nabla\mathbf{u}_r^{k+1}\|\|\nabla\boldsymbol{\eta}^{k+1}\|^2 \\
&\overset{(3.39)}{\le} \left(\nu^{-1/2}|||\mathbf{f}|||_{2,-1} + ||\mathbf{u}_r^0||\right)\Delta t\sum_{k=0}^{M-1}\|\nabla\mathbf{u}_r^{k+1}\|\|\nabla\boldsymbol{\eta}^{k+1}\|^2
\end{aligned}$$

$$\overset{(3.31)}{\leq} C\left(\nu^{-1/2}|||\mathbf{f}|||_{2,-1} + ||\mathbf{u}_r^0||\right)\Delta t \sum_{k=0}^{M-1} \|\nabla \mathbf{u}_r^{k+1}\|(h^{2m} + ||S_r||_2 h^{2m+2} + (1 + ||S_r||_2)\,\Delta t^2 + \sum_{j=r+1}^{d} ||\boldsymbol{\varphi}_j||_1^2 \lambda_j). \tag{3.60}$$

We note that we used estimate (3.31) in the derivation of (3.60); using (3.25) would not have been enough for the asymptotic convergence of (3.60).

The fifth term on the RHS of (3.57) can be bounded as follows:

$$\Delta t \sum_{k=0}^{M-1} \|\nabla \mathbf{u}^{k+1}\|^2 \|\nabla \boldsymbol{\eta}^{k+1}\|^2$$

$$\overset{(3.31)}{\leq} C\Delta t \sum_{k=0}^{M-1} \|\nabla \mathbf{u}^{k+1}\|^2 (h^{2m} + ||S_r||_2 h^{2m+2} + (1 + ||S_r||_2)\,\Delta t^2 + \sum_{j=r+1}^{d} ||\boldsymbol{\varphi}_j||_1^2 \lambda_j). \tag{3.61}$$

Since in (3.53) q_h was an arbitrary function in Q^h, we can use the approximation property (3.17) in Assumption 3.1 to bound the seventh term on the RHS of (3.57) as follows:

$$\Delta t \sum_{k=0}^{M-1} \|p - q_h\|^2 \leq C h^{2m}. \tag{3.62}$$

Using (2.2c), we have the following error bound of the last term on the RHS of (3.57):

$$\Delta t \sum_{k=0}^{M-1} \|P_R' \nabla \mathbf{u}^{k+1}\|^2 = \Delta t \sum_{k=0}^{M-1} \|\nabla \mathbf{u}^{k+1} - P_R \nabla \mathbf{u}^{k+1}\|^2$$

$$\leq C \frac{1}{M} \sum_{k=0}^{M-1} \inf_{\mathbf{v}_R \in \mathbf{X}^R} \|\nabla \mathbf{u}^{k+1} - \nabla \mathbf{v}_R\|^2 \leq C \frac{1}{M} \sum_{k=0}^{M-1} \|\nabla \mathbf{u}^{k+1} - \nabla \mathbf{w}_R^{k+1}\|^2$$

$$\overset{(3.25)}{\leq} C\left(h^{2m} + ||S_R||_2 h^{2m+2} + (1 + ||S_R||_2)\,\Delta t^2 + \sum_{j=R+1}^{d} ||\boldsymbol{\varphi}_j||_1^2 \lambda_j\right). \tag{3.63}$$

Collecting (3.58)–(3.63) and letting $d = C(6\nu + 2\alpha) + 6C^3\nu^{-1}(\nu^{-\frac{1}{2}}|||f|||_{2,-1} + ||\mathbf{u}_r^0||)|||\nabla \mathbf{u}_r|||_{1,0} + 6C^3\nu^{-1}|||\nabla \mathbf{u}_r|||_{2,0}^2$, $d_1 = \frac{C^4 9^3 \nu^{-3}}{2}$, $d_2 = 6C\nu^{-1}(\|\mathbf{u}_{tt}\|_{2,2}^2 + 1) + 2C\alpha + d$, $d_3 = 6C\nu^{-1} + 2C\alpha + d$, and $d_4 = 2\alpha C$, Eq. (3.57) becomes

$$\|\phi_r^M\|^2 + \nu\Delta t \sum_{k=0}^{M-1} \|\nabla \phi_r^{k+1}\|^2 + \alpha\Delta t \sum_{k=0}^{M-1} \|P_R' \nabla \phi_r^{k+1}\|^2$$

$$\leq d_1 \Delta t \sum_{k=0}^{M-1} \|\nabla \mathbf{u}^{k+1}\|^4 \|\phi_r^{k+1}\|^2 + d_2 \Delta t^2 + d||S_r||_2 \Delta t^2 + d_3 h^{2m} + d||S_r||_2 h^{2m+2}$$

$$+ d \sum_{j=r+1}^{d} ||\boldsymbol{\varphi}_j||_1^2 \lambda_j + d_4 \left(||S_R||_2 \Delta t^2 + ||S_R||_2 h^{2m+2} + \sum_{j=R+1}^{d} ||\boldsymbol{\varphi}_j||_1^2 \lambda_j\right). \tag{3.64}$$

If $\Delta t < \Delta t^* := d_1 |||\nabla \mathbf{u}|||_{4,0}^4$, the discrete Gronwall lemma (see Lemma 27 in [18] and also [32]) implies the following inequality:

$$\begin{aligned}
&\|\phi_r^M\|^2 + \nu \Delta t \sum_{k=0}^{M-1} \|\nabla \phi_r^{k+1}\|^2 + \alpha \Delta t \sum_{k=0}^{M-1} \|P_R' \nabla \phi_r^{k+1}\|^2 \\
&\quad \leq C^* (d_2 \Delta t^2 + d ||S_r||_2 \Delta t^2 + d_3 h^{2m} + d ||S_r||_2 h^{2m+2} + d \sum_{j=r+1}^{d} ||\boldsymbol{\varphi}_j||_1^2 \lambda_j \\
&\qquad + d_4 (||S_R||_2 \Delta t^2 + ||S_R||_2 h^{2m+2} + \sum_{j=R+1}^{d} ||\boldsymbol{\varphi}_j||_1^2 \lambda_j)),
\end{aligned} \tag{3.65}$$

where $C^* = e^{d_1 \Delta t \sum_{k=0}^{M-1} \left\|\nabla \mathbf{u}^{k+1}\right\|^4}$.

By dropping the third term on the LHS of (3.65) and using (3.30), (3.25), and the triangle inequality, we get

$$\begin{aligned}
&\left\|\mathbf{u}^M - \mathbf{u}_r^M\right\|^2 + \nu \Delta t \sum_{k=0}^{M-1} \left\|\nabla \left(\mathbf{u}^{k+1} - \mathbf{u}_r^{k+1}\right)\right\|^2 \\
&\quad \leq C ((1 + ||S_r||_2 + ||S_R||_2) \Delta t^2 + h^{2m} + (1 + ||S_r||_2 + ||S_R||_2) h^{2m+2} \\
&\qquad + \sum_{j=r+1}^{d} \left(1 + ||\boldsymbol{\varphi}_j||_1^2\right) \lambda_j + \sum_{j=R+1}^{d} ||\boldsymbol{\varphi}_j||_1^2 \lambda_j).
\end{aligned} \tag{3.66}$$

This completes the proof. ∎

IV. NUMERICAL EXPERIMENTS

The goal of this section is twofold. In Section IV.A, we investigate the physical accuracy of the P_R -VMS-POD-ROM. To this end, we test the model in the numerical simulation of a 3D flow past a circular cylinder at $\mathrm{Re} = 1000$. The P_R -VMS-POD-ROM is compared with the POD-G-ROM and the ML-POD-ROM in which a constant EV is used [6, 7]. All the numerical results are benchmarked against DNS data. A parallel CFD solver is used to generate the DNS data [36]. For details on the numerical discretization, the reader is referred to the appendix in [37]. To assess the physical accuracy of the POD-ROMs, two criteria are used: (i) the time evolution of the POD coefficients, which measures the instantaneous behavior of the models; and (ii) the energy spectrum, which measures the average behavior of the models. In Section IV.B, we illustrate numerically the theoretical error estimates in Theorem 3.1. Specifically, we investigate the error's asymptotic behavior with respect to the time step, Δt, and the POD contribution to the error introduced by the EV term, $\sum_{j=R+1}^{d} ||\boldsymbol{\varphi}_j||_1^2 \lambda_j$.

A. Physical Accuracy

In this section, we test the P_R -VMS-POD-ROM in the numerical simulation of a 3D flow past a circular cylinder at $\mathrm{Re} = 1000$. By using the method of snapshots [3], we compute the POD basis $\{\varphi_1, \cdots, \varphi_d\}$ from 1000 snapshots of the velocity field over 15 shedding cycles, that is, $t \in [0, 75]$

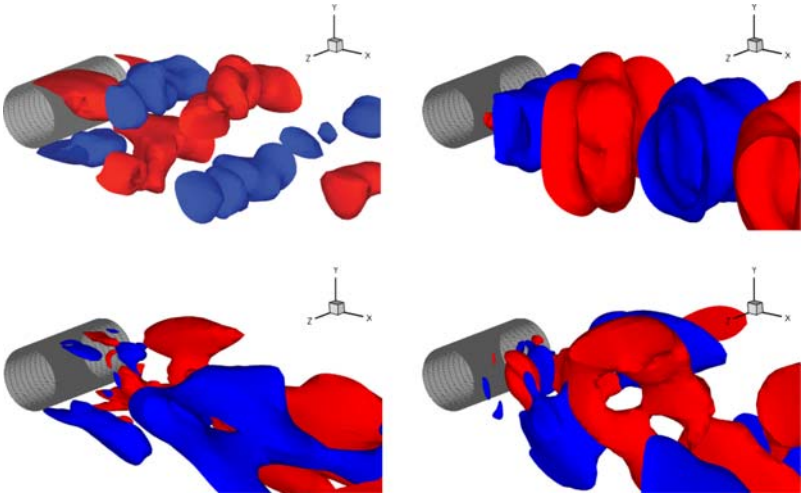

FIG. 1. 3D flow past a cylinder at Re = 1000. First streamwise POD mode (top left), first normal POD mode (top right), third streamwise POD mode (bottom left), and third normal POD mode (bottom right). [Color figure can be viewed in the online issue, which is available at wileyonlinelibrary.com.]

(see Fig. 1). These POD modes are then interpolated onto a structured quadratic FE mesh with nodes coinciding with the nodes used in the original DNS finite volume discretization. Six POD basis functions ($r = 6$) are then used in all POD-ROMs that we investigate next. These first six POD modes capture 84% of the system's energy. For all these POD-ROMs, the time discretization was effected by using the backward Euler method with $\Delta t = 7.5 \times 10^{-3}$. We emphasize that the time interval used in the simulations of POD-ROMs is four times larger than that in which snapshots are generated, that is, $t \in [0, 300]$. Thus, the predictive capabilities of the POD-ROMs are investigated. In Fig. 2, the time evolutions of the POD coefficients a_1 and a_4 are plotted. The other POD coefficients have a similar qualitative behavior, so, for clarity, they are not included in our plots. To determine the EV constants in the ML-POD-ROM and the P_R -VMS-POD-ROM, we run the models on the short time interval [0, 15] with several different values for the EV constants and choose the value that yields the results that are closest to the DNS results. This approach yields the following values for the EV constants: $\alpha = 3 \times 10^{-3}$ for the ML-POD-ROM (2.14) and $\alpha = 3.5 \times 10^{-3}$ for the P_R-VMS-POD-ROM (2.12) when $R = 1$. We emphasize that these EV constant values are optimal only on the short time interval tested, and they might actually be nonoptimal on the entire time interval [0, 300] on which the POD-ROMs are tested. Thus, this heuristic procedure ensures some fairness in the numerical comparison of the three POD-ROMs.

The POD-G-ROM (2.10) performs poorly, although it is computationally efficient (its CPU time is 118s). Indeed, the amplitude of the temporal evolution of the POD coefficient $a_4(\cdot)$ is nine times larger than that for the DNS projection. The ML-POD-ROM's time evolutions of the POD coefficients a_1 and a_4 are also inaccurate. Specifically, although the time evolution at the beginning of the simulation (where the EV constant α was chosen) is relatively accurate, the accuracy significantly degrades toward the end of the simulation. For example, as shown in Fig. 2(b), the magnitude of a_4 at the end of the simulation is only one eighth of that of the DNS. The P_R -VMS-POD-ROM yields more accurate time evolutions than both the POD-G-ROM and the ML-POD-ROM for both a_1 and a_4, as shown in Fig. 2(c). The P_R -VMS-POD-ROM is as efficient as POD-G-ROM, its CPU time being 129 s.

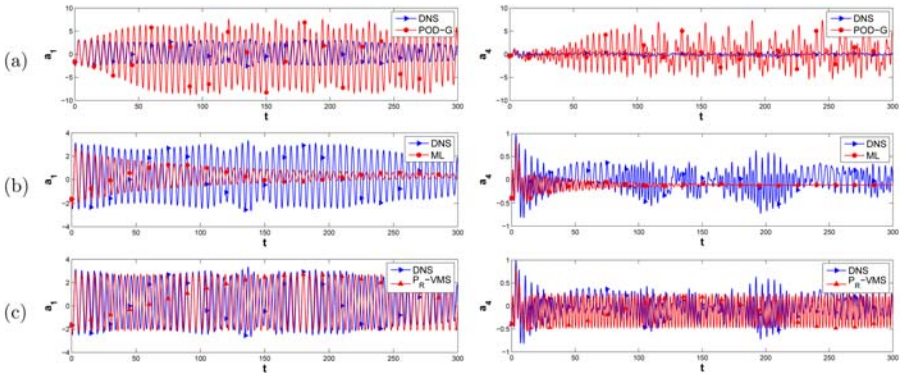

FIG. 2. 3D flow past a cylinder at Re = 1000. Temporal evolution of POD coefficients $a_1(\cdot)$ and $a_4(\cdot)$ over the time interval [0, 300] for POD-G-ROM (a), ML-POD-ROM (b), and P_R-VMS-POD-ROM (c). [Color figure can be viewed in the online issue, which is available at wileyonlinelibrary.com.]

Figure 3 presents the energy spectra of the three POD-ROMs. The three energy spectra are compared with the DNS energy spectrum. For the energy spectra, we use the approach in [7] and we calculate the average kinetic energy of the nodes in the cube with side 0.1 centered at the probe (0.9992, 0.3575, 1.0625). The energy spectrum of the POD-G-ROM (2.10) overestimates the energy spectrum of the DNS. The energy spectrum of the ML-POD-ROM (2.14), conversely, underestimates the energy spectrum of the DNS, especially at the higher frequencies. Although it displays high oscillations at the higher frequencies, the P_R -VMS-POD-ROM (2.12) has a more accurate spectrum than both the POD-G-ROM (2.10) and the ML-POD-ROM (2.14).

B. Numerical Accuracy

In this section, we test the P_R -VMS-POD-ROM in the numerical simulation of the 2D incompressible NSE (2.1). The exact velocity, $\mathbf{u} = (u, v)$, has components $u = \frac{2}{\pi}\arctan(-500(y-t))\sin(\pi y)$, $v = \frac{2}{\pi}\arctan(-500(x-t))\sin(\pi x)$, and the exact pressure is given by $p = 0$. The inverse of the Reynolds number is $\nu = 10^{-3}$ and the forcing term is chosen to match the exact solution.

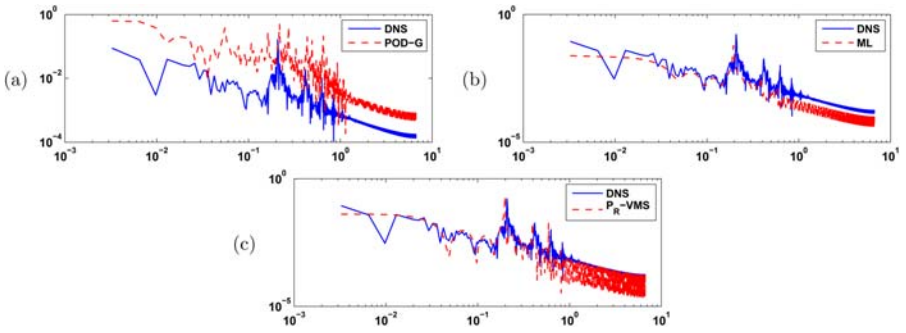

FIG. 3. 3D flow past a cylinder at Re = 1000. Comparison of energy spectrum of DNS with that of POD-G-ROM (a), ML-POD-ROM (b), and P_R-VMS-POD-ROM (c). [Color figure can be viewed in the online issue, which is available at wileyonlinelibrary.com.]

TABLE I. The P_R-VMS-POD-ROM with $h = 1/64$, $r = 99$, $R = 95$, and $\alpha = 10^{-3}$. The error $\mathcal{E}$ for decreasing values of the time step, Δt.

Δt	$\mathcal{E}$
1×10^{-2}	5.97×10^{-2}
5×10^{-3}	3.19×10^{-2}
2.5×10^{-3}	1.38×10^{-2}
1.25×10^{-3}	9.38×10^{-3}

Taylor-Hood FEs are used to discretize the spatial domain $[0, 1] \times [0, 1]$. We collect snapshots over the time interval [0, 1] at every $\Delta T = 10^{-2}$ by recording the exact values of u and v on the FE mesh with the mesh size $h = 1/64$. After applying the method of snapshots, we obtain a POD basis set with the dimension of 101.

In POD-ROMs, the backward Euler method is used for time integration over the same time interval. To verify the numerical error of the P_R -VMS-POD-ROM (2.12) with respect to the time step, Δt, we choose $h = 1/64$, $r = 99$, $R = 95$ and $\alpha = 10^{-3}$. With this choice, h^{2m} is on the order of 10^{-8}, and $\sum_{j=r+1}^{d} ||\boldsymbol{\varphi}_j||_1^2 \lambda_j$ and $\sum_{j=R+1}^{d} ||\boldsymbol{\varphi}_j||_1^2 \lambda_j$ are on the order of 10^{-4}. Thus, asymptotically, the time discretization error dominates the total error in the theoretical error estimate (3.40). The error $\mathcal{E} = \sqrt{||\mathbf{u}^M - \mathbf{u}_r^M||^2 + \nu \Delta t \sum_{k=0}^{M-1} \|\nabla \left(\mathbf{u}^{k+1} - \mathbf{u}_r^{k+1}\right)\|^2}$ is listed in Table I for decreasing values of the time step, Δt. A linear regression (see Fig. 4) indicates an almost linear correlation between the error $\mathcal{E}$ and the time step Δt:

$$\mathcal{E} = 4.05(\Delta t)^{0.92},$$

which is close to the linear approximation property predicted by the theoretical error estimate (3.40).

To verify the numerical error of the P_R -VMS-POD-ROM with respect to R, we choose $h = 1/64$, $\Delta t = 10^{-4}$, and $r = 99$. With this choice, h^{2m} and Δt^2 are on the order of

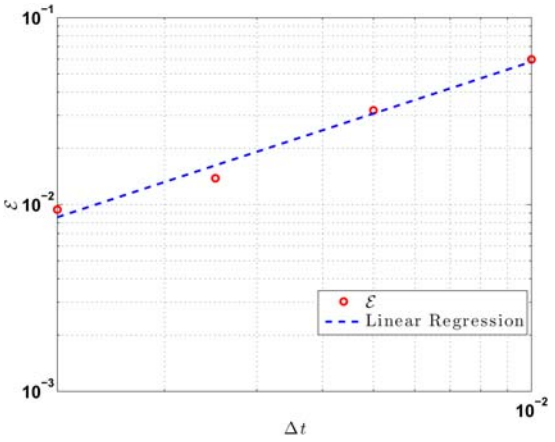

FIG. 4. The P_R-VMS-POD-ROM with $h = 1/64$, $r = 99$, $R = 95$ and $\alpha = 10^{-3}$. A linear regression between the total error in the L^2 norm at the final time, $\mathcal{E}$, and the time step, Δt, is nearly linear: $\mathcal{E} \sim \mathcal{O}\left((\Delta t)^{0.92}\right)$. [Color figure can be viewed in the online issue, which is available at wileyonlinelibrary.com.]

TABLE II. The P_R-VMS-POD-ROM with $h = 1/64$, $\Delta t = 10^{-4}$, $r = 99$, and $\alpha = 10^{-3}$. The approximate error $\mathcal{E}$ for increasing values of R.

R	$\sqrt{\sum_{j=R+1}^{d} \|\|\boldsymbol{\varphi}_j\|\|_1^2 \lambda_j}$	$\mathcal{E}$
6	14.7	1.70×10^{-2}
10	14.1	1.59×10^{-2}
16	13.1	1.47×10^{-2}
24	11.9	1.37×10^{-2}

10^{-8} and $\sum_{j=r+1}^{d} ||\boldsymbol{\varphi}_j||_1^2 \lambda_j$ is on the order of 10^{-4}. Thus, asymptotically, the POD contribution to the error introduced by the EV term, $\sum_{j=R+1}^{d} ||\boldsymbol{\varphi}_j||_1^2 \lambda_j$, dominates the total error in the theoretical error estimate (3.40). For a fixed $\alpha = 10^{-3}$, the error $\mathcal{E} = \sqrt{||\mathbf{u}^M - \mathbf{u}_r^M||^2 + \nu \Delta t \sum_{k=0}^{M-1} \|\nabla \left(\mathbf{u}^{k+1} - \mathbf{u}_r^{k+1}\right)\|^2}$ is listed in Table II for increasing values of R. A linear regression between $\mathcal{E}$ and $\sqrt{\sum_{j=R+1}^{d} ||\boldsymbol{\varphi}_j||_1^2 \lambda_j}$ (see Fig. 5) shows a nearly linear correlation between the considered terms:

$$\mathcal{E} = 1.03 \times 10^{-3} \left(\sqrt{\sum_{j=R+1}^{d} ||\boldsymbol{\varphi}_j||_1^2 \lambda_j} \right)^{1.04},$$

which is close to the linear approximation property predicted by the theoretical error estimate (3.40).

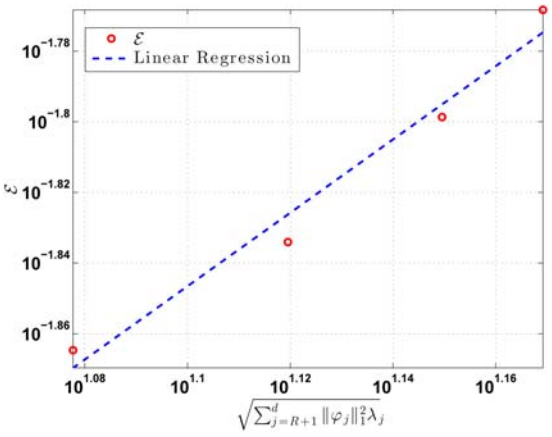

FIG. 5. The P_R-VMS-POD-ROM with $h = 1/64$, $\Delta t = 10^{-4}$, $r = 99$, and $\alpha = 10^{-3}$. A linear regression between the error $\mathcal{E}$ and the POD contribution to the error introduced by the EV term: $\mathcal{E} \sim \mathcal{O}\left(\left(\sqrt{\sum_{j=R+1}^{d} ||\boldsymbol{\varphi}_j||_1^2 \lambda_j}\right)^{1.04}\right)$. [Color figure can be viewed in the online issue, which is available at wileyonlinelibrary.com.]

V. CONCLUSIONS

In this article, we proposed a new ROM for the numerical simulation of turbulent incompressible fluid flows. This model, denoted P_R -VMS-POD-ROM, utilizes a VMS method and a projection operator to model the effect of the high index POD modes that are not included in the ROM. Under two assumptions on the underlying FE approximation and the generation of the POD basis, an error estimate was derived for the full discretization of the P_R -VMS-POD-ROM. All the contributions to the total error were considered: the spatial discretization error (due to the FE discretization), the temporal discretization error (due to the backward Euler method), and the POD truncation error. The P_R -VMS-POD-ROM was also tested in the numerical simulation of a 3D flow past a circular cylinder at $Re = 1000$. The numerical tests showed that the P_R -VMS-POD-ROM is both physically accurate and computationally efficient. Furthermore, the numerical results illustrated the theoretical error estimates.

We note that the EV coefficient α in the P_R -VMS-POD-ROM is simply chosen to be a constant. We plan to extend this theoretical and numerical study by considering more accurate choices for the EV coefficients, such as the Smagorinsky model [7, 38]. We also plan to investigate this model in more complex physical settings, such as the Boussinesq equations [39]. Finally, we plan to reduce the computational cost of the P_R -VMS-POD-ROM by a different treatment of the time discretization of the VMS term.

The authors thank the anonymous reviewers for their constructive comments, which helped improve the manuscript.

References

1. J. A. Atwell and B. B. King, Reduced order controllers for spatially distributed systems via proper orthogonal decomposition, SIAM J Sci Comput 26 (2004), 128–151.
2. J. L. Lumley, The structure of inhomogeneous turbulent flows, Atmospheric Turbulence and Radio Wave Propagation, Nauka, Moscow 1967, pp. 166–178.
3. L. Sirovich, Turbulence and the dynamics of coherent structures. I. coherent structures, Q Appl Math 45 (1987), 561–571.
4. L. Sirovich, Turbulence and the dynamics of coherent structures. II. symmetries and transformations, Q Appl Math 45 (1987), 573–582.
5. L. Sirovich, Turbulence and the dynamics of coherent structures. III. dynamics and scaling, Q Appl Math 45 (1987), 583–590.
6. N. Aubry, P. Holmes, J. L. Lumley, and E. Stone, The dynamics of coherent structures in the wall region of a turbulent boundary layer, J Fluid Mech 192 (1988), 115–173.
7. Z. Wang, I. Akhtar, J. Borggaard, and T. Iliescu, Proper orthogonal decomposition closure models for turbulent flows: a numerical comparison, Comput Methods Appl Mech Eng 237–240 (2012), 10–26.
8. T. J. R. Hughes, L. Mazzei, A. Oberai, and A. Wray, The multiscale formulation of large eddy simulation: decay of homogeneous isotropic turbulence, Phys Fluids 13 (2001), 505–512.
9. T. J. R. Hughes, A. Oberai, and L. Mazzei, Large eddy simulation of turbulent channel flows by the variational multiscale method, Phys Fluids 13 (2001), 1784–1799.
10. T. Iliescu and Z. Wang, Variational multiscale proper orthogonal decomposition: convection-dominated convection-diffusion-reaction equations, Math Comput 82 (2013), 1357–1378.
11. V. John and S. Kaya, A finite element variational multiscale method for the Navier–Stokes equations, SIAM J Sci Comput 26 (2005), 1485–1503.

12. V. John and S. Kaya, Finite element error analysis of a variational multiscale method for the Navier-Stokes equations, Adv Comput Math 28 (2008), 43–61.

13. V. John, S. Kaya, and A. Kindl, Finite element error analysis for a projection-based variational multiscale method with nonlinear eddy viscosity, J Math Anal Appl 344 (2008), 627–641.

14. V. John, S. Kaya, and W. Layton, A two-level variational multiscale method for convection-dominated convection-diffusion equations, Comput Methods Appl Mech Eng 195 (2006), 4594–4603.

15. W. J. Layton, A connection between subgrid scale eddy viscosity and mixed methods, Appl Math Comput 133 (2002), 147–157.

16. J.-L. Guermond, Stabilization of Galerkin approximations of transport equations by subgrid modeling. M2AN, Math Model Numer Anal 33 (1999), 1293–1316.

17. J.-L. Guermond, Stablisation par viscosité de sous-maille pour l'approximation de Galerkin des opérateurs linéaires monotones, Comptes Rendus Serie Sciences Mathenatiques 328 (1999), 617–622.

18. W. J. Layton, Introduction to the numerical analysis of incompressible viscous flows, Vol. 6, Society for Industrial and Applied Mathematics (SIAM), Philadelphia, USA, 2008.

19. K. Kunisch and S. Volkwein, Galerkin proper orthogonal decomposition methods for parabolic problems, Numer Math 90 (2001), 117–148.

20. D. Chapelle, A. Gariah, and J. Sainte-Marie, Galerkin approximation with proper orthogonal decomposition: new error estimates and illustrative examples, ESAIM Math Model Numer Anal 46 (2012), 731–757.

21. P. Holmes, J. L. Lumley, and G. Berkooz, Turbulence, coherent structures, dynamical systems and symmetry, Cambridge University Press, Cambridge, UK, 1996.

22. J. R. Singler, New POD error expressions, error bounds, and asymptotic results for reduced order models of parabolic PDEs, to appear.

23. S. Volkwein, Model reduction using proper orthogonal decomposition, 2011. Available at: http://www.math.uni-konstanz.de/numerik/personen/volkwein/teaching/POD-Vorlesung.pdf. Accessed on 11 November, 2013.

24. K. Kunisch and S. Volkwein, Galerkin proper orthogonal decomposition methods for a general equation in fluid dynamics, SIAM J Numer Anal 40 (2002), 492–515.

25. Z. Luo, J. Chen, I. M. Navon, and X. Yang, Mixed finite element formulation and error estimates based on proper orthogonal decomposition for the nonstationary Navier-Stokes equations, SIAM J Numer Anal 47 (2008), 1–19.

26. V. Girault and P.-A. Raviart, Finite element approximation of the Navier-Stokes equations, Vol. 749, Lecture notes in mathematics, Springer-Verlag, Berlin, 1979.

27. T. Geveci, On the convergence of a time discretization scheme for the Navier-Stokes equations, Math Comput 53 (1989), 43–53.

28. J. G. Heywood and R. Rannacher, Finite element approximation of the nonstationary Navier-Stokes problem, part II: stability of solutions and error estimates uniform in time, SIAM J Numer Anal 23 (1986), 750–777.

29. R. Rannacher, Stable finite element solutions to nonlinear parabolic problems of Navier-Stokes type, R. Glowinski and J. L. Lions, editors, North-Holland, Amsterdam, 1982, pp. 301–309.

30. G. A. Baker, Galerkin approximations for the Navier-Stokes equations, Technical Report, Harvard University, 1976.

31. G. A. Baker, V. Dougalis, and O Karakashian, On a higher order accurate fully discrete Galerkin approximation to the Navier-Stokes equations, Math Comput 39 (1982), 339–375.

32. J. G. Heywood and R. Rannacher, Finite-element approximation of the nonstationary Navier-Stokes problem, part IV: error analysis for second-order time discretization, SIAM J Numer Anal 27 (1990), 353–384.

33. L. C. Berselli, T. Iliescu, and W. J. Layton, Mathematics of large eddy simulation of turbulent flows, Scientific Computation, Springer-Verlag, Berlin, 2006.

34. C. Foiaş, O. Manley, R. Rosa, and R. Temam, Navier-Stokes equations and turbulence, Cambridge University Press, New York, USA, 2001.

35. K. Kunisch and S. Volkwein, Control of the Burgers equation by a reduced-order approach using proper orthogonal decomposition, J Optim Theory Appl 102 (1999), 345–371.

36. I. Akhtar, Parallel simulations, reduced-order modeling, and feedback control of vortex shedding using fluidic actuators, PhD thesis, Virginia Tech, Blacksburg, USA, 2008.

37. Z. Wang, I. Akhtar, J. Borggaard, and T. Iliescu, Two-level discretizations of nonlinear closure models for proper orthogonal decomposition, J Comput Phys 230 (2011), 126–146.

38. S. Ullmann and J. Lang, A POD-Galerkin reduced model with updated coefficients for Smagorinsky LES, J. C. F. Pereira and A. Sequeira, editors, V European conference on computational fluid dynamics, ECCOMAS CFD 2010, Lisbon, Portugal, June 2010.

39. S. S. Ravindran, Error analysis for Galerkin POD approximation of the nonstationary Boussinesq equations, Numer Methods Partial Differ Equat 27 (2010), 1639–1665.